

Integration of auto-steering with adaptive cruise control for improved cornering behaviour

Idriz, Adem Ferad; Abdul Rachman, Arya Senna; Baldi, Simone

DOI

[10.1049/iet-its.2017.0089](https://doi.org/10.1049/iet-its.2017.0089)

Publication date

2017

Document Version

Accepted author manuscript

Published in

IET Intelligent Transport Systems

Citation (APA)

Idriz, A. F., Abdul Rachman, A. S., & Baldi, S. (2017). Integration of auto-steering with adaptive cruise control for improved cornering behaviour. *IET Intelligent Transport Systems*, 11(10), 667-675. <https://doi.org/10.1049/iet-its.2017.0089>

Important note

To cite this publication, please use the final published version (if applicable). Please check the document version above.

Copyright

Other than for strictly personal use, it is not permitted to download, forward or distribute the text or part of it, without the consent of the author(s) and/or copyright holder(s), unless the work is under an open content license such as Creative Commons.

Takedown policy

Please contact us and provide details if you believe this document breaches copyrights. We will remove access to the work immediately and investigate your claim.

Integration of Auto-Steering with Adaptive Cruise Control for Improved Cornering Behavior

Adem F. Idriz¹, Arya S. Abdul Rachman² ✉, Simone Baldi³

^{1 2 3} Delft Center for System and Control, Delft University of Technology, Mekelweg 2, Delft, the Netherlands

✉ E-mail: me@AryaSenna.web.id

Abstract: Several works have proposed longitudinal control strategies enabling a vehicle to operate adaptive cruise control and collision avoidance functions. However, no integration with lateral control has been proposed in the current state of the art, which motivates the developments of this work. This paper presents an integrated control strategy for adaptive cruise control with auto-steering for highway driving. An appropriate logic-based control strategy is used to create synergies and safe interaction between longitudinal and lateral controllers to obtain both lateral stability and advanced adaptive cruise control functionalities. In particular, an index is proposed to evaluate lateral motion of the vehicle based on previously published experimental studies on human driving. In order to handle unstable lateral motion of the vehicle, the desired acceleration is determined based on physical limitation in braking with cornering situations. Simulation results show that the proposed integrated controller satisfies the performance in terms of autonomous driving, path tracking and collision avoidance for various driving situations.

1 Introduction

An advanced driver assistance systems is a vehicle control system that uses environment sensors (e.g. radar, laser, vision, GPS) to improve driving comfort and traffic safety by assisting the driver in recognizing and reacting to potentially dangerous traffic situations [1]. To improve handling performance and active safety of vehicles, a considerable number of advanced driver assistance systems for vehicle lateral dynamics and longitudinal collision-safety have been developed and utilized commercially over the last two decades. For example, Cruise Control (CC), Adaptive Cruise Control (ACC), Collision Avoidance (CA) have been extensively researched [2]. However, the vast majority of systems proposed in literature [3–7] is focused on longitudinal control with minimal or no focus on lateral control. As a result, the major drawback of commercially available longitudinal control systems is the limited performance in cornering situations [8].

Since the vehicle longitudinal and lateral motions are naturally coupled, it is recognized that the integration of longitudinal and lateral control, also referred to as Integrated Vehicle Dynamics Control (IVDC) [9, 10], presents some challenges due to the co-existence of several control subsystems that can cause increased complexity and conflicts of control objectives and actions. Although the definition of IVDC is still under discussion, its attributes are evident, i.e. it needs to coordinate two or more subsystems systematically according to control objectives and actions [11]. The lack of integrated lateral and longitudinal control might lead in the worst case to conflicting actions, so that the resulting performance might be worse than the performance of longitudinal-only or lateral-only control [2]. Moreover, coordinated control of the actuators is necessary to obtain both lateral stability and safe clearance of autonomous driving vehicle, and also to avoid rear-end collisions in severe driving situations.

In literature, it has been proposed to use the vehicle body side-slip angle and yaw moment respectively to sense the lateral motion of the vehicle and to ensure the lateral stability by controlling these terms [2, 5]. To support integration, most researchers tend to adopt a multi-layer control structure in charge of the coordination and distribution of subsystems [4]. However, note that no specific integration logic (e.g. threshold values for the desired yaw moment and the error in slip angle) has been suggested so far. Furthermore, human factor issues have been widely acknowledged to play a key role in IVDC effectiveness [12]: the design of IVDC based on human driving behaviour

encourages better driver acceptance [13] and increases safety [14]. However, to the best of the authors' knowledge, there exists no experimental study on human driving concerning the desired yaw moment and the error in slip angle.

In this paper, a novel IVDC is proposed that creates safe interaction between longitudinal and lateral controllers. The proposed IVDC aims to avoid rear-end collision and unstable lateral motion of the vehicle. In particular, in severe driving situations, the proposed control strategy is designed based on longitudinal and lateral indices for driving situations to coordinate the braking and steering actuators. Since the vehicle slip angle is not directly measurable by sensors, we propose a novel lateral index based on previously published experimental studies on human driving concerning lateral acceleration levels. We focus on highway driving scenarios. Note that this approach does not require differential braking, thus allowing the use of a two-wheeled vehicle model (bicycle model) which is typically adopted in ACC applications for low computational complexity and real-time control.

Simulations are conducted in Matlab/Simulink by using a set of highway traffic scenarios which are likely to occur in reality. Simulation results show that the proposed integrated controller satisfies the performance in terms of autonomous driving and collision avoidance.

The paper is structured as follows: Section 1 introduces vehicle dynamics and the longitudinal controller design, while the lateral controller is discussed in Section 3. Section 4 describes the integrated control structure. Simulations are conducted in Section 5 and conclusions are presented in Section 6. All units in the equations are understood to be SI units (so velocities are in m s^{-1} and angles are in rad).

2 Longitudinal control design

The longitudinal control strategy adopted in this work is presented together with some basics on vehicle dynamics, which will be used for control purposes.

2.1 Vehicle Dynamics

We consider a 3-Degree of Freedom vehicle model, accounting for the two displacements on the plane (longitudinal, indicated with subscript x , and lateral, indicated with subscript y) and the rotation around an axis normal to the plane (yaw rotation). Assuming that the vehicle

travels at constant speed and that the turning radius is much larger than the vehicle's track width, the two-wheeled vehicle model [15], can be written as

$$ma_x = mv_y\dot{\psi} + \cos\delta F_{x,f} + F_{x,r} - \sin\delta F_{y,f} - F_e \quad (1)$$

$$ma_y = -mv_x\dot{\psi} + \cos\delta F_{y,f} + F_{y,r} + \sin\delta F_{x,f} \quad (2)$$

$$I_z\ddot{\psi} = l_f \cos\delta F_{y,f} - l_r F_{y,r} + l_f \sin\delta F_{x,f} \quad (3)$$

where $F_{x,f}$ and $F_{y,f}$ are the longitudinal and lateral tire forces for front wheels, $F_{x,r}$ and $F_{y,r}$ are the longitudinal and lateral tire forces for rear wheels, δ is the front wheel steering angles, F_e includes lumped external forces (aerodynamic drag force, rolling resistance force and gravitational resistance force due to road slope), l_f and l_r are respectively the distance from the vehicle Centre of Gravity (CoG) to the front and the rear wheel axle of the vehicle, m is the total mass of the vehicle, v_x and v_y are longitudinal and lateral velocity of the host (ACC-equipped) vehicle, a_x and a_y are the longitudinal and lateral acceleration of the host vehicle, I_z is the mass moment of inertia with respect to a vertical axis, ψ and $\dot{\psi}$ are yaw angle and yaw rate of the host vehicle. We use the well-known Pacejka formula [16] for longitudinal tire forces

$$\begin{aligned} \mu(s_i) &= D_P \sin(C_P \arctan(B_P s_i - E_P(B_P s_i \\ &\quad - \arctan(B_P s_i)))) \\ F_{x,i} &= \mu(s_i) F_{z,i} \end{aligned} \quad (4)$$

where the subscript $i = f, r$ denotes the front and rear wheel respectively, s_i are the longitudinal wheel-slip ratios, $\mu(\cdot)$ is the slip ratio dependent friction coefficient, B_P , C_P , D_P , E_P are the coefficients depending on the road surface, $F_{z,i}$ are the normal forces exerting on the wheels. For the purpose of this study, we concentrate on the dry tarmac (asphalt).

The lateral tire forces are assumed to be linear functions of slip angles α_i and cornering stiffness C_{y_i} [17]

$$F_{y,i} = 2C_{y,i}\alpha_i. \quad (5)$$

As commonly assumed in literature, we consider that longitudinal and lateral tire forces are limited physically by the adhesion limit between tire and road defined by Kamm circle [18, Sect. 13.8]

$$\sqrt{F_{y,i}^2 + F_{x,i}^2} \leq \mu F_{z,i}. \quad (6)$$

2.2 Longitudinal control modes

The longitudinal controller, aiming at maintaining the longitudinal motion of the vehicle, consists of an upper-level and a low-level controller, as shown in Fig. 1a. The upper-level controller computes the desired acceleration required to attain the desired spacing or velocity. The computed acceleration command is transmitted to the low-level controller that calculates the corresponding actuation commands (throttle and brake). Here we elaborate more on the upper-level controller, while for the low-level controller, the interested reader is referred to the classic approaches presented in [4, 7].

The upper-level longitudinal control scheme is the one typically adopted in the literature [19] and consisting of four modes (CC, ACC, ACC+CA and CA), as depicted in Fig. 1b. In this work the CC mode implements a proportional-derivative control [15]

$$\begin{aligned} e_v &= v_x - v_{set} \\ a_{x,M0} &= K_p e_v + K_d \frac{de_v}{dt} \end{aligned} \quad (7)$$

where v_{set} is the velocity of the host vehicle set by the driver. The first term in (7) represents the proportional action and the second term is the derivative action. Since an ideal derivative is not causal, the implementation of the PD controller (7) will include an additional

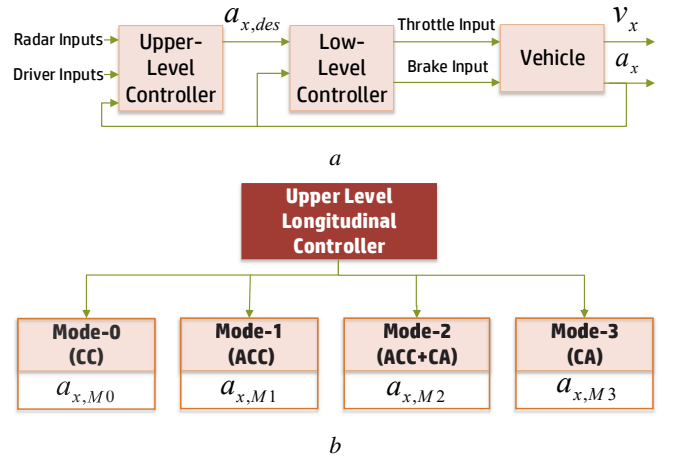


Fig. 1: Longitudinal Controller

(a) Hierarchy diagram (b) Control modes of upper-level.

low-pass filtering for the derivative term to limit the high-frequency gain and noise [18, Sect. 5.3]. The other three modes (ACC, ACC+CA and CA) are implemented via a linear-quadratic controller consisting of index-based scheduling of acceleration as proposed in [6]

$$d_{des} = d_0 + v_x t_{hw}$$

$$v_{rel} = v_{x,t} - v_x, \quad e_d = d - d_{des}$$

$$a_{x,M1} = K_e e_d + K_v v_{rel} \quad (8)$$

$$a_{x,M2} = \max \left\{ a_{x,M1}, -4 \text{ ms}^{-2} \right\} \quad (9)$$

$$a_{x,M3} = \max \left\{ a_{x,M1}, -\mu g \text{ ms}^{-2} \right\} \quad (10)$$

where d_0 is a constant representing the desired distance at standstill, t_{hw} is the desired headway time, d is the distance between the host and target vehicles as measured by the radar, $v_{x,t}$ is the velocity of the target vehicle, and v_{rel} is the relative velocity between vehicles, and K_e , K_v are the gains of the linear-quadratic controller. As shown in Algorithm 1, one of the four modes is activated depending on d , on a warning index κ , and on an inverse Time To Collision (TTC^{-1}) index

$$\kappa = \frac{d - d_b}{d_w - d_b}, \quad \text{TTC}^{-1} = \frac{v_{rel}}{d}. \quad (11)$$

Algorithm 1 Longitudinal Mode Determination

- 1: **if** $d > \bar{d}$ **then**
- 2: **use** $a_{x,M0}$
- 3: **else if** $d \leq \bar{d}$ **and** $(\kappa \geq \bar{\kappa} \text{ and } \text{TTC}^{-1} \leq \bar{T})$ **then**
- 4: **use** $a_{x,M1}$
- 5: **else if** $d \leq \bar{d}$ **and** $(\kappa \leq \bar{\kappa} \text{ or } \text{TTC}^{-1} > \bar{T})$ **then**
- 6: **use** $a_{x,M2}$
- 7: **else if** $d \leq \bar{d}$ **and** $(\kappa \leq \underline{\kappa} \text{ or } \text{TTC}^{-1} \geq \bar{T})$ **then**
- 8: **use** $a_{x,M3}$
- 9: **end if**

In Algorithm 1, \bar{d} is a design parameter (with $\bar{d} \geq d_{des}$, e.g. $\bar{d} = 1.5d_{des}$) indicating the maximum error distance beyond which CC is switched on. Note that that \bar{d} should be selected by taking into account the distance beyond which the radar cannot detect any target vehicle (typically around 200 m): if d is larger than the maximum radar operating range, by definition d is not available and we operate in CC mode. The parameters d_b and d_w in (11) are the braking-critical

and warning-critical distances, defined as

$$\begin{aligned} d_b &= \frac{v_x^2 - (v_x - v_{rel})^2}{2\mu g} \\ d_w &= \frac{v_x^2 - (v_x - v_{rel})^2}{2\mu g} + v_{rel}\tau_h \end{aligned} \quad (12)$$

and derived from the kinematics of two vehicles that brake to a full stop [6]: τ_h is the typical human response delay. Finally, $\underline{\kappa}$, $\bar{\kappa}$, \underline{T} , \bar{T} are user defined thresholds. Note that no integration of the longitudinal control (7)-(10) with lateral control has been proposed in the current state of the art, which motivates the development presented in the next subsection.

2.3 Vehicle Stability Control

Together with CC, ACC, ACC+CA, and CA, an additional Vehicle Stability Control (VSC) mode is designed with the aim to improve vehicle lateral motion and keep the vehicle on the desired path (e.g. the test circuits in Fig. 2b). This is done by calculating a desired longitudinal acceleration $a_{x,des}$ from physical limitation in braking with cornering situation

$$a_{x,VSC} = -\frac{\sqrt{(\mu mg)^2 - (\sum F_y)^2}}{m}. \quad (13)$$

The rationale behind (13) is the following: substitute in (6) the longitudinal forces with $ma_{x,des}$ and the normal forces with μmg , so as to obtain the deceleration (13). In this way, the constraint on longitudinal acceleration is tightened by using the Kamm inequality (6). Note that F_y in (13) must be either estimated [20, 21], or it can be even measured by using recently developed technology like smart tires [22] or load sensing bearings [23].

The next steps will be then to design a steering angle control (which will be done in Sect. 3) and to design a safe interaction between the longitudinal accelerations (7)-(10), (13) and the steering angle control (which will be done in Sect. 4).

3 Lateral control design

Lateral control involves the steering of the vehicle, so as to maintain the host vehicle in the centre of the lane: in this work, lane keeping is modeled as a path tracking problem.

3.1 Linearized Model

By adopting the classical two-degree of freedom vehicle model, the lateral position error y_r is defined as the lateral distance between the CoG and the centre-line of the desired path (see Fig. 2a). Yaw angle error is denoted with ε and defined as the difference between the yaw angle of the vehicle ψ and the desired yaw angle as dictated by the desired path ψ_d . The rate of changes of the lateral position error and the yaw angle error are defined as [17]

$$\dot{y}_r = v_y + v_x\varepsilon, \quad \varepsilon = \psi - \psi_d \quad (14)$$

$$\dot{\psi}_d = \frac{v_x}{\rho} \quad (15)$$

where ρ denotes the radius of curvature of the desired path (see Fig. 2b for two examples). Assuming that the lateral tire force is linearly related to the side slip angle by the cornering stiffness as in (5), the tire side-slip angles can be rewritten as

$$F_{y,f} = C_{y,f}\alpha_f, \quad F_{y,r} = C_{y,r}\alpha_r. \quad (16)$$

By using small angle approximation for steering angle (less than 5 degrees for highway driving situations), the tire angle is [17]

$$\alpha_f = \delta - \left(\frac{v_y + l_f\dot{\psi}}{v_x} \right), \quad \alpha_r = - \left(\frac{v_y - l_r\dot{\psi}}{v_x} \right). \quad (17)$$

The lateral tire forces can be expressed by substituting (14) and (15) into (5)

$$F_{y,f} = 2C_{y,f} \left[\delta - \left(\frac{\dot{y}_r + l_f\dot{\varepsilon}}{v_x} \right) + \varepsilon - \frac{l_f}{v_x}\dot{\psi}_d \right] \quad (18)$$

$$F_{y,r} = 2C_{y,r} \left[- \left(\frac{\dot{y}_r - l_r\dot{\varepsilon}}{v_x} \right) + \varepsilon + \frac{l_r}{v_x}\dot{\psi}_d \right]. \quad (19)$$

The dynamic behavior of the steering actuator is approximated by a first-order lag element [24]

$$\tau_\delta\dot{\delta} + \delta = \delta_{des} \quad (20)$$

where τ_δ denotes the dynamic time constant and δ_{des} the desired wheel steering angle. Finally, lateral dynamic equations are obtained by substituting (20), (18) and (19) into (2) and (3).

$$\begin{aligned} \dot{\chi}_y &= A_y\chi_y + B_yu_y + \Gamma_yw_y \\ \chi_y &= [y_r \quad \dot{y}_r \quad \varepsilon \quad \dot{\varepsilon} \quad \delta]^T \end{aligned} \quad (21)$$

with matrices

$$A_y = \begin{bmatrix} 0 & 1 & 0 & 0 & 0 \\ 0 & \frac{\alpha_{y,1}}{v_x} & -a_{y,1} & \frac{\alpha_{y,2}}{v_x} & a_{y,5} \\ 0 & 0 & 0 & 0 & 0 \\ 0 & \frac{\alpha_{y,3}}{v_x} & -a_{y,3} & \frac{\alpha_{y,4}}{v_x} & a_{y,6} \\ 0 & 0 & 0 & 0 & -\frac{1}{\tau_\delta} \end{bmatrix} \quad B_y = \begin{bmatrix} 0 \\ 0 \\ 0 \\ 0 \\ \frac{1}{\tau_\delta} \end{bmatrix} \quad (22)$$

$$\Gamma_y = \begin{bmatrix} 0 & 0 \\ 1 & 0 \\ 0 & 0 \\ 0 & 1 \\ 0 & 0 \end{bmatrix} \quad w_y = \begin{bmatrix} w_{y,1} \\ w_{y,2} \end{bmatrix} \quad (23)$$

$$\begin{aligned} a_{y,1} &= \frac{-2(C_{y,f} + C_{y,r})}{m} & a_{y,2} &= \frac{2(-l_fC_{y,f} + l_rC_{y,r})}{m} \\ a_{y,3} &= \frac{2(-l_fC_{y,f} + l_rC_{y,r})}{I_z} & a_{y,4} &= \frac{-2(l_f^2C_{y,f} + l_r^2C_{y,r})}{I_z} \\ a_{y,5} &= \frac{2C_{y,f}}{m} & a_{y,6} &= \frac{2l_fC_{y,f}}{I_z} \\ w_{y,1} &= \frac{-v_x^2}{\rho} + \frac{\alpha_{y,2}}{v_x}\dot{\psi}_d & w_{y,2} &= \frac{\alpha_{y,4}}{v_x}\dot{\psi}_d - \ddot{\psi}_d \end{aligned}$$

where the disturbance term w_y is defined from road information (ρ , $\dot{\psi}_d$, $\ddot{\psi}_d$). Note that, in contrast with [17], one extra state δ appears in (21). The extra state comes from the steering dynamics (18) so that the control exploits the information about the actuation authority.

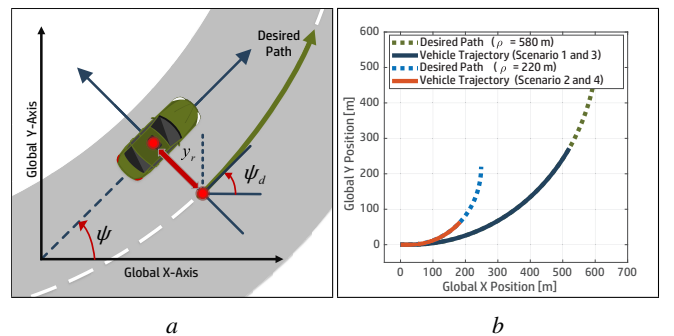


Fig. 2: Vehicle movement in reference frame
(a) Yaw and lateral error, (b) Test circuits (with different radius of curvature ρ)

3.2 Steering Controller

Following a similar approach as in [17], an optimal finite preview control method is used to develop a steering controller. The intention is to eliminate lateral and yaw angle error through a combination of feedback and feed-forward control. The feedback control input of the steering controller for path-tracking is computed using lateral position error and yaw angle error. The feed-forward control input is computed using the road information within the preview distance.

The steering control input is computed to minimize the performance index [17]

$$J_y(\chi_y, \lambda, t) = \int_0^\infty \left(\frac{1}{2} \chi_y^T Q_y \chi_y + \frac{1}{2} \delta_{des}^T R_y \delta_{des} + \dots \right. \\ \left. \dots \lambda^T (A_y \chi_y + B_y \delta_{des} + \Gamma_y w_y - \dot{\chi}_y) \right) dt \quad (23)$$

where R_y is a positive scalar and Q_y a positive semidefinite matrix defined as follows

$$Q_y = \begin{bmatrix} Q_{y_r} & 0 & 0 & 0 & 0 \\ 0 & Q_{\dot{y}_r} & 0 & 0 & 0 \\ 0 & 0 & Q_\varepsilon & 0 & 0 \\ 0 & 0 & 0 & Q_{\dot{\varepsilon}} & 0 \\ 0 & 0 & 0 & 0 & Q_\delta \end{bmatrix}. \quad (24)$$

As a result, the steering control input is computed as

$$\delta_{des}(t) = -K_y \chi_y(t) + M(t) \quad (25)$$

where the Lagrangian multiplier λ is calculated as in [25] using the form

$$\lambda(t) = P_y(t) \chi_y(t) + H(t)$$

with $P_y(t)$ is the solution of Riccati equation and $H(t)$ satisfies

$$\dot{H} = -A_c^T H - P_y \Gamma_y w_y, \quad A_c = A_y - B_y R_y^{-1} B_y^T P_y. \quad (26)$$

Consider a preview time T_p , which is a function of v_x and ρ , obtained from experiments on human factors [26]. By using the road information between time t and $t + T_p$, (26) becomes

$$H(t, T_p) = \int_t^{t+T_p} (e^{-A_c^T(t-\tau)} P_{y,ss} \Gamma_y w_y(t)) d\tau \quad (27)$$

and thus, the steering control input is used to minimize the cost function where K_y is the optimal feedback gain, $M(t)$ is the finite preview control term, which are given as

$$K_y = -R_y^{-1} B_y^T P_y, \quad M(t) = -R_y^{-1} B_y^T H(t, T_p). \quad (28)$$

4 Integrated Control Design

In this section, previously designed longitudinal and lateral controllers are integrated into a novel Integrated Vehicle Dynamics Control (IVDC), shown in Fig. 3.

The proposed integration scheme consists of two main functionalities, namely determination of desired and comfort speed, and index-based control. In addition, the commands are delivered to the throttle, brake and steering actuators by the low-level controller.

4.1 Desired and comfort speed determination

The determination of comfort speed is essential so that the lateral acceleration of the host vehicle does not exceed a critical value: in fact, for high lateral accelerations, vehicle model goes non-linear and controlling the vehicle becomes more difficult.

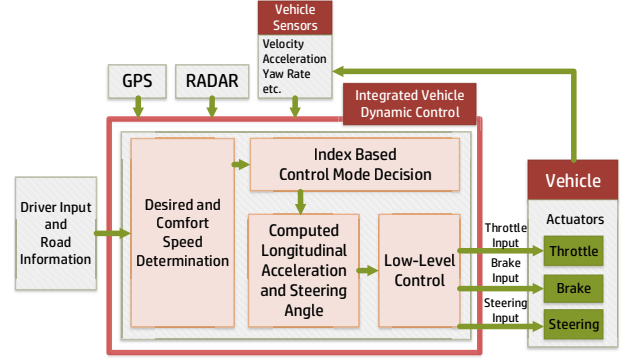


Fig. 3: Scheme of multi-layer integrated vehicle dynamics control system

Therefore, based on human comfort experiments published in [27], the absolute value of lateral acceleration is limited via velocity-dependent constraints as

$$|a_{y,des}(v_x)| = a_{y,0} \left(1 - \frac{v_x}{v_{max}} \right), \quad 0 \leq v_x \leq v_{max} \quad (29)$$

$$v_{comfort} = \sqrt{\rho |a_{y,des}(v_x)|} \quad (30)$$

where $a_{y,0}$ is the acceptable lateral acceleration in highways (also called medium comfort-level lateral acceleration), $a_{y,des}$ is the desired lateral acceleration of the host vehicle, $v_{comfort}$ is the desired velocity of the host vehicle in the terms of comfort in curve, g is the gravitational acceleration, v_{max} is the maximum speed of the host vehicle. Note that (29) decreases linearly and monotonically for higher velocities.

The desired velocity of the host vehicle v_{des} results in

$$v_{set} \leq v_{limit} = \sqrt{\rho g \mu} \quad (31)$$

$$v_{des} = \min \{ v_{set}, v_{comfort} \} \quad (32)$$

where (31) is a requirement for the user, being v_{set} as in (7), and v_{limit} the maximum allowable velocity in curve beyond which the vehicle is driven away from the curve. The rationale behind (29)-(32) is the following: experimental studies on human driving show that drivers tend to have lower lateral acceleration values at higher speeds: so, a velocity-dependent lateral comfort constraint is designed in view of human comfort. The absolute value of desired lateral acceleration is determined in (29): then, $v_{comfort}$ is calculated in (30) based on the radius of curve and $a_{y,des}$. The vehicle is not allowed to reach higher speed than v_{limit} in (31) due to centripetal force, where v_{limit} determines a constraint on the user-set velocity as in (32).

4.2 Index-based control plane

A task of the decision layer is to determine which one of five control modes (CC, ACC, ACC+CA, CA, or VSC) to activate.

The activation of the five modes is based on an appropriately designed index plane that uses longitudinal and lateral indices. Fig. 4a shows the proposed index-plane. The index-plane consists of a "Normal Driving Mode", an "Integrated Safety Mode I", and an "Integrated Safety Mode II". Integrated safety modes are used to avoid collision and unstable lateral motion of the vehicle.

Similar to [2], the longitudinal index I_{long} is determined by using a warning index and an inverse TTC

$$I_{long} = f_1(\kappa) + f_2(\text{TTC}^{-1}) \quad (33)$$

where $f_1(\cdot)$ is a positive piecewise linear function of the warning index κ and $f_2(\cdot)$ is a positive piecewise linear function of the inverse

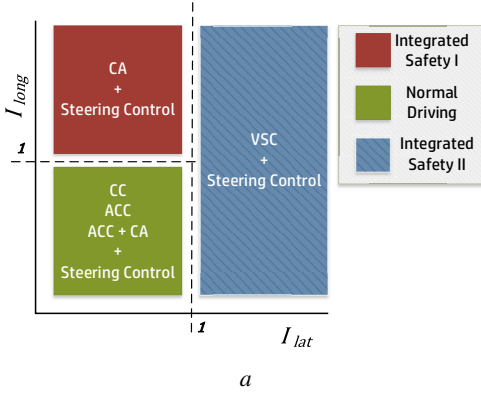


Fig. 4: Index-based plane: (a) Integrated mode, (b) Longitudinal index, (c) Lateral index.

time to collision. The combination of the two functions gives rise to the piecewise linear function represented in Fig. 4b. In this work, we propose a novel lateral index I_{lat}

$$a_{y,max}(v_x) = \mu g \left(1 - \frac{v_x}{v_{max}} \right), \quad I_{lat} = \frac{|a_y|}{a_{y,max}(v_x)} \quad (34)$$

where a_y is the lateral acceleration of the host vehicle and $a_{y,max}$ is the velocity-dependent maximum value of lateral acceleration. The proposed lateral index is based on experimental studies on human driving [27], which showed that values above $a_{y,max}$ definitely cause discomfort for human driving and also complicate the control of a vehicle. Note that $a_{y,max}$ decrease linearly as the velocity increases. The index I_{lat} is represented in Fig. 4c.

Summarizing (cf. Algorithm 2):

- In "Normal Driving Mode", which covers CC, ACC, and ACC + CA, the desired longitudinal acceleration $a_{x,des}$ is determined as $a_{x,M0}$ (7), $a_{x,M1}$ (8), or $a_{x,M2}$ (9), depending on the active longitudinal mode;
- In "Integrated Safety Mode I", which covers CA, the desired longitudinal acceleration $a_{x,des}$ is determined as $a_{x,M3}$ (10);
- In "Integrated Safety Mode II", the VSC mode with acceleration (13) has priority over all the other modes, i.e. the desired longitudinal acceleration is $a_{x,des} = a_{x,VSC}$. Note that this extra mode provides a safe interaction between longitudinal acceleration and steering angle control, as demonstrated in the evaluation section.
- Finally, the desired steering angle δ_{des} is determined (no matter which mode is active) by using (25).

Algorithm 2 Integrated Mode Determination

- 1: **if** $I_{long} < 1$ **and** $I_{lat} < 1$ **then**
 - 2: Normal Driving Mode is active
 - 3: **else if** $I_{long} \geq 1$ **and** $I_{lat} < 1$ **then**
 - 4: Integrated Safety Mode I is active
 - 5: **else if** $I_{lat} \geq 1$ **then**
 - 6: Integrated Safety Mode II is active
 - 7: **end if**
-

Remark. *The objective of proposed index-based integration is to satisfy both longitudinal safety and lateral stability. If the longitudinal index exceeds unit, the danger of collision is high; if the lateral index exceeds unit, the danger of unstable lateral motion is high. Notice that in the "Integrated Safety Mode I", the longitudinal safety control has priority to avoid rear-end collision; while in the "Integrated Safety Mode II", the lateral stability control has priority to improve vehicle lateral motion.*

4.3 Low-level control

Based on the desired longitudinal acceleration and steering angle, the low-level control manipulates throttle, brake and steering actuators. The steering angle obtained from (25) is transmitted directly to the steering actuator; the throttle/brake actuator input depends on the low-level controller as in [4, 7].

5 Evaluation

For the evaluation of the designed integrated control system, several test scenarios are determined for various traffic situations, including the decentralized scenario in which the integrated control system is not present. We focus on highway driving scenarios. The performance specifications (steady-state errors) are defined as follows:

- for longitudinal control we consider (Table 1a): the steady-state value of e_d (spacing error), i.e. the steady-state distance error between the desired distance and the actual distance; the steady-state value of v_{rel} , i.e. the steady-state relative velocity between target and host vehicle;
- for lateral control we consider (Table 1b): the steady-state value of y_r , i.e. the steady-state lateral position error; the steady-state value of ε , i.e. the steady-state yaw angle error.

The term steady-state indicates a value that is reached, after some transient, on a straight road or on a path with constant curvature.

With the exception of scenario 3, all simulations run with headway time of 1.5s. For all simulations, the proposed controller is activated after 1s from the beginning of the simulation, in order to start from a non trivial initial state and allow the internal states of the vehicle model and of the low-level controller to reach a meaningful working point. Simulations are conducted on MATLAB/Simulink [28]. Relevant parameters can be found in Tables 2, 3 and 4. For more complete simulations, the interested reader is referred to the demonstration video [29], conducted on the vehicle simulator Dynacar [30].

Table 1 Performance specifications:

(a) Longitudinal		(b) Lateral	
	a		b
Performance Spec.	Criteria	Performance Spec.	Criteria
$ e_d $ ACC at steady-state	≤ 0.5 m	$ y_r $ at steady-state	≤ 0.2 m
$ v_{rel} $ ACC at steady-state	≤ 1.0 m s ⁻¹	$ \varepsilon $ at steady-state	≤ 0.02 rad

Test Scenario 1: Integrated Safety I

This test scenario is dedicated to examine longitudinal safety control performance in case of possible rear-end collision. The host and target vehicle drive on a test circuit consisting of a 30 m straight line

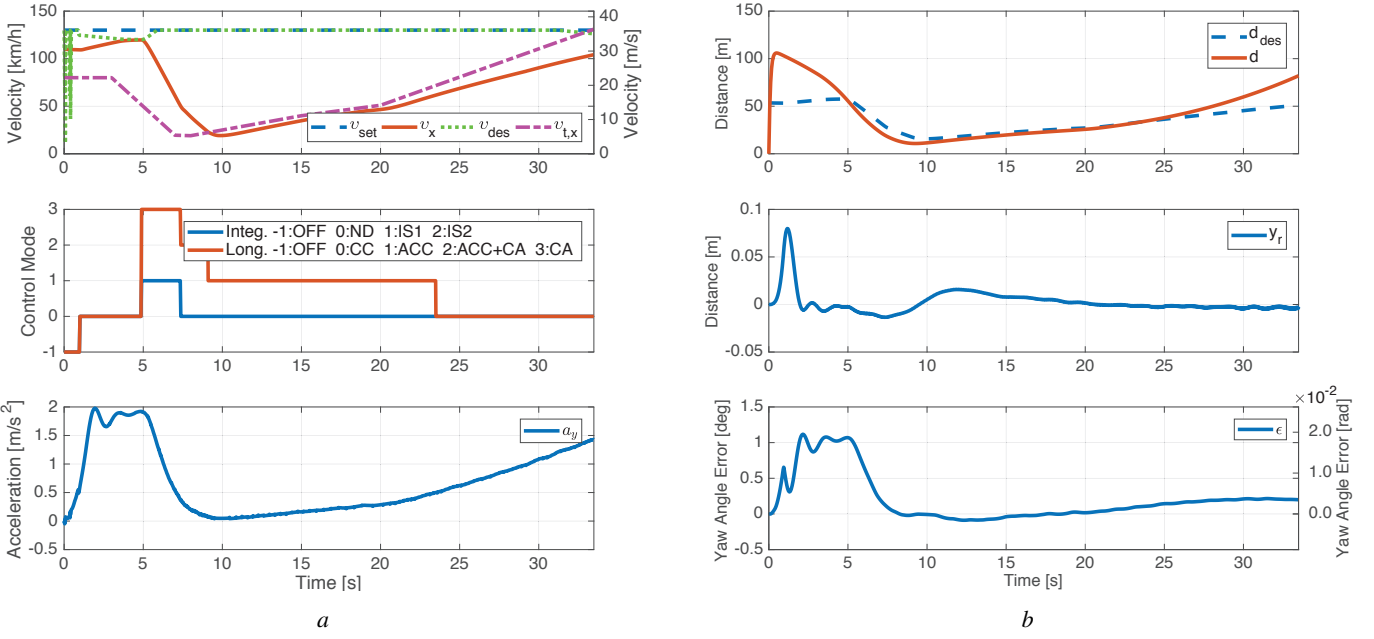


Fig. 5: Results for scenario 1: (a) Velocity, mode, lateral accelerations (b) Distance, lateral position, yaw angle error.

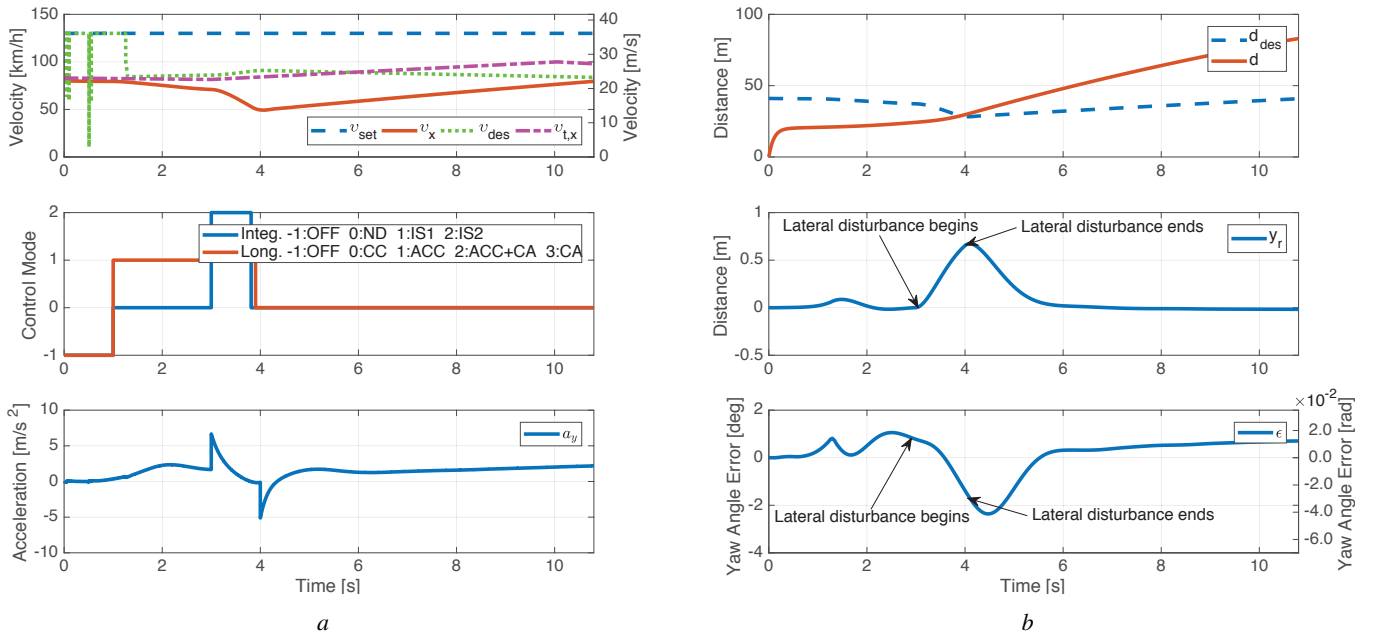
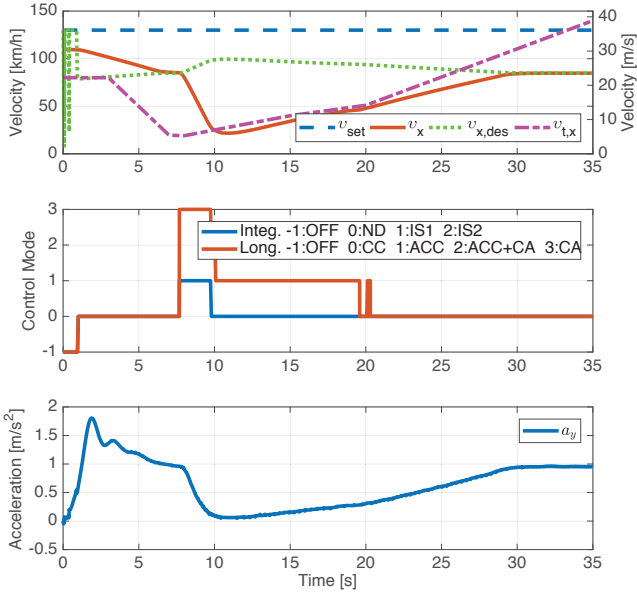


Fig. 6: Results for scenario 2: (a) Velocity, mode, lateral accelerations (b) Distance, lateral position, yaw angle error.

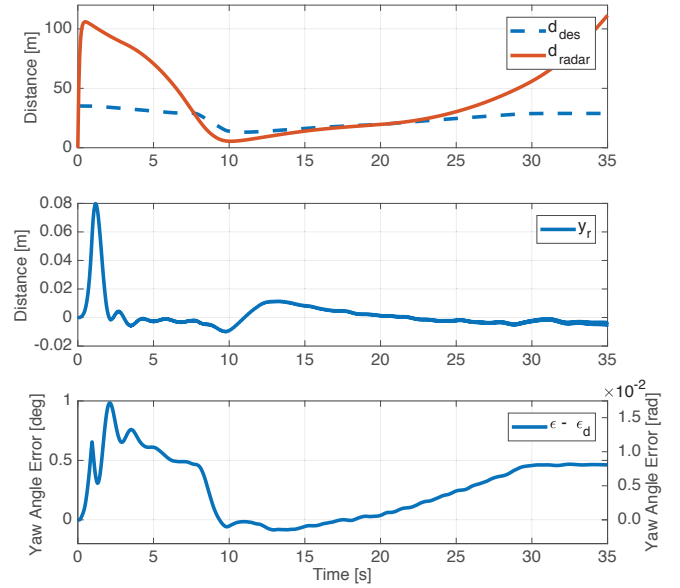
and a curve with 580 m radius (cf. Fig. 2b). The target vehicle starts to decelerate at 3 s during cornering. The integrated control system recognizes the target vehicle as dangerous based on the warning index and the inverse TTC, and severe braking is applied in order to avoid collision with the target vehicle. After 20 s, the target vehicle starts to accelerate fast, and since the acceleration of the host vehicle is limited for passenger comfort, the system enables the CC mode. Integrated and longitudinal control modes shown in Fig. 5a indicate that longitudinal safety control to avoid rear-end collision has priority in the current driving situation. Despite the priority of longitudinal control, Fig. 5b reveals that lateral stability is maintained since lateral position and yaw angle errors are kept small during the whole simulation.

Test Scenario 2: Integrated Safety II

This test scenario investigates lateral safety control when the host and target vehicle run on a test circuit consisting of a 30 m straight line and a curve with 220 m radius (cf. Fig. 2b). The scenario has been constructed in such a way that an external force of magnitude 7125 N is applied laterally to the centre of gravity of the vehicle between 3 s to 4 s, i.e. simulating another vehicle bumping sideways. As a consequence of this disturbance, the lateral index exceeds 1 (possible unstable lateral motion) and Integrated Safety II mode is triggered as displayed in Fig. 6a. The braking and steering inputs are simultaneously applied to the vehicle to track the desired path while maintaining lateral stability. It can be observed that, except for the time interval in which the vehicle is subject to the disturbance, lateral



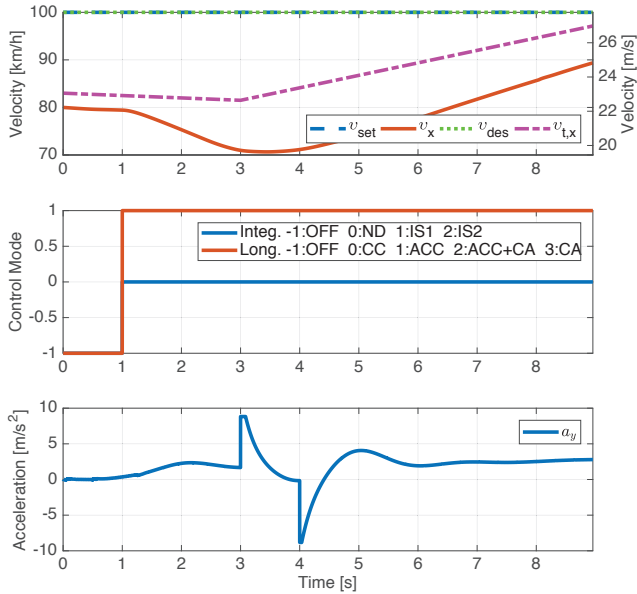
a



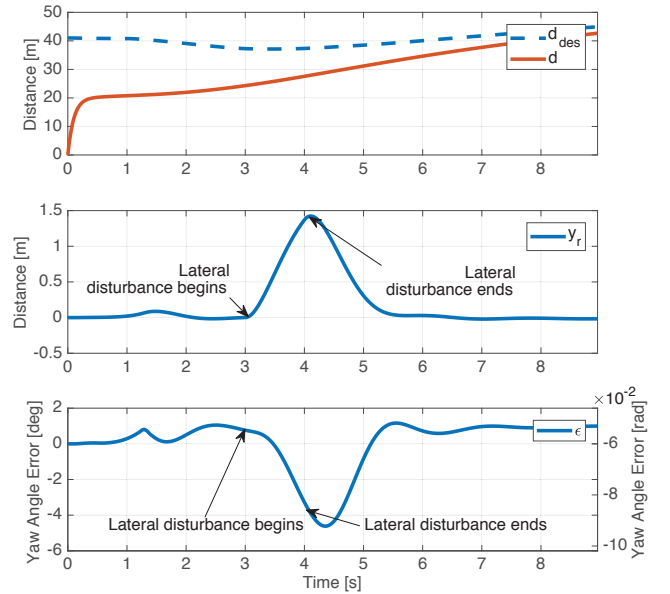
b

Fig. 7: Results for scenario 3:

(a) Velocity, mode, lateral accelerations (b) Distance, lateral position, yaw angle error.



a



b

Fig. 8: Results for scenario 4:

(a) Velocity, mode, lateral accelerations, (b) Distance, lateral position, yaw angle error.

acceleration does not exceed comfort limits. Fig. 6b shows that the steering angle reacts immediately to reject the disturbance. The magnitudes of lateral position and yaw angle errors are within acceptable bounds. Overall, the proposed integrated controller handles unstable lateral vehicle motion adequately and quickly.

Test Scenario 3: Integrated Safety I with decreased headway time

This scenario runs on the same track and with the same target vehicle as scenario 1, but with a smaller headway time of 0.8s (almost half of the default headway time). The purpose is to check the reliability of the proposed scheme in safety-critical situations. Remind that the typical headway time for ACC systems is somewhere between 1

and 2 seconds, and that smaller headway can be achieved only via cooperative adaptive cruise control implementations. As a result, a headway time of 0.8s might be beyond the design limit of most ACC systems [31]. Similar to scenario 1, Fig. 7a and Fig. 7b indicate that severe braking is applied in order to avoid collision with the target vehicle. The collision is avoided, after which the CC mode is enabled, as in scenario 1.

Test Scenario 4: No Integrated Safety II, Lateral Control isolated from Longitudinal Control

In this scenario, the effect of decentralized (not integrated) vehicle dynamics control is examined. Without integrated safety, the longitudinal and lateral control are decentralized. The track is the same as in

scenario 2. Similarly, the same external force of magnitude 7125 N is applied laterally to the centre of gravity of the vehicle between 3 s to 4 s, i.e. simulating another vehicle bumping sideways. However, due to lack of any integration, the Integrated Safety II mode is not triggered, as displayed in Fig. 8a. As a result, the VSC mode is not activated, and it can be seen that lateral acceleration is much larger than in scenario 2 (approximately 2 times larger, cf. Fig. 6a and Fig. 8a): also lateral displacement and yaw angle error are almost twice as large as in scenario 2 (cf. Fig. 6b and Fig. 8b). It can be observed that without the integrated controller, excessive oversteering occurs and the values of lateral acceleration far exceeds the discomfort level [27]. In realistic situation, these conditions are potentially hazardous: the vehicle could end up being outside its own lane, and when roll dynamics [18] is taken into account, the risk of rollover is heightened.

6 Conclusions

An integrated control system has been proposed by appropriately interconnecting longitudinal and lateral controllers. It consists of an index-based decision plane to create synergy and safe interaction between longitudinal and lateral controllers to ensure better overall performance. Simulations have been conducted in order to investigate the performance of the proposed IVDC system in various driving situations. From the simulations, it has been shown that the proposed system achieves lateral stability and prevents the vehicle to vehicle collision. In particular, the integrated controller which coordinates both longitudinal and lateral motions augments the safety of vehicle in severe driving situation.

Future works will include real-time implementation of integrated controller and experimental verification, integration of a function for friction coefficient estimation, integration of advanced algorithms for driving manoeuvres such overtaking or lane change, and Cooperative ACC systems with vehicle-to-vehicle communication.

7 Acknowledgment

This research has been partially sponsored by the Dutch Automated Vehicle Initiative (DAVI), website: <http://davi.connekt.nl/>

8 References

- Gietlink, O., Ploeg, J., Schutter, B.D., Verhaegen, M.: 'Development of advanced driver assistance systems with vehicle hardware-in-the-loop simulations', *Vehicle System Dynamics*, 2006, **44**, (7), pp. 569–590
- Cho, W., Heo, H., Yi, K., Moon, S., Lee, C.: 'Design and Evaluation of an Integrated Vehicle Safety System for Longitudinal Safety and Lateral Stability'. In: 22nd Int. Tech. Conf. Enhanc. Saf. Veh., 2011, pp. 1–9
- Reschka, A., Böhrer, J.R., Saust, F., Lichte, B., Maurer, M.: 'Safe, dynamic and comfortable longitudinal control for an autonomous vehicle', *IEEE Intell Veh Symp Proc*, 2012, pp. 346–351
- Yi, K., Lee, S., Kwon, Y.D.: 'An investigation of intelligent cruise control laws for passenger vehicles', *Proc Inst Mech Eng Part D J Automob Eng*, 2001, **215**, (2), pp. 159–169
- Naus, G.J.L., Ploeg, J., Van de Molengraft, M.J.G., Heemels, W.P.M.H., Steinbuch, M.: 'Design and implementation of parameterized adaptive cruise control: An explicit model predictive control approach', *Control Eng Pract*, 2010, **18**, (8), pp. 882–892
- Moon, S., Moon, I., Yi, K.: 'Design, tuning, and evaluation of a full-range adaptive cruise control system with collision avoidance', *Control Eng Pract*, 2009, **17**, (4), pp. 442–455
- Eyisi, E., Zhang, Z., Koutsoukos, X., Porter, J., Karsai, G., Sztipanovits, J.: 'Model-based control design and integration of cyberphysical systems: An adaptive cruise control case study', *Hindawi Publishing Corporation Journal of Control Science and Engineering*, 2013, pp. 1–15
- Kim, D., Moon, S., Park, J., Kim, H.J., Yi, K.: 'Design of an adaptive cruise control / collision avoidance with lane change support for vehicle autonomous driving', 2009.
- Attia, R., Orjuela, R., Basset, M.: 'Combined longitudinal and lateral control for automated vehicle guidance', *Veh Syst Dyn*, 2014, **52**, (2), pp. 261–279
- Nilsson, J., Brannstrom, M., Fredriksson, J., Coelingh, E.: 'Longitudinal and Lateral Control for Automated Yielding Maneuvers', *IEEE Trans Intell Transp Syst*, 2016, **17**, (5), pp. 1404–1414
- Yu, F., Li, D., Crolla, D.A.: 'Integrated vehicle dynamics control-state-of-the-art review', *IEEE Vehicle Power and Propulsion Conference (VPPC)*, September, 2008, pp. 3–5
- Vahidi, A., Eskandarian, A.: 'Research advances in intelligent collision avoidance and adaptive cruise control', *IEEE Trans Intell Transp Syst*, 2003, **4**, (3), pp. 143–153
- Hoedemaeker, M.: 'Driving with intelligent vehicles: Driving behaviour with ACC and the acceptance by individual drivers', *Proc IEEE Intell Transp Syst Conf*, 2000, pp. 506–509
- Marsden, G., McDonald, M., Brackstone, M.: 'Towards an understanding of adaptive cruise control', *Transp Res Part C Emerg Technol*, 2001, **9**, (1), pp. 33–51
- Guvenç, B.A., Kural, E.: 'A low-cost, multiple-driver-in-the-loop adaptive cruise control simulator', 2006, pp. 42–55
- Laila, D.S., Shakouri, P., Ordys, A., Askari, M.: 'Longitudinal vehicle dynamics using simulink/matlab'. In: UKACC Int. Conf. Control 2010, 2010, pp. 955–960
- Kang, J., Hindiyeh, R.Y., Moon, S., Gerdes, J.C., Yi, K.: 'Design and testing of a controller for autonomous vehicle path tracking using gps/ins sensors'. In: Proceedings of the 17th World Congress of IFAC Seoul, Korea, 2008, pp. 6–11
- Rajamani, R.: 'Vehicle Dynamics and Control'. Mechanical Engineering Series. (Boston, MA: Springer US, 2012)
- Shakouri, P., Ordys, A.: 'Nonlinear model predictive control approach in design of adaptive cruise control with automated switching to cruise control', *Control Engineering Practice*, 2014, **26**, pp. 160–177
- Cho, W., Yoon, J., Yim, S., Koo, B., Yi, K.: 'Estimation of tire forces for application to vehicle stability control', *IEEE Transactions on Vehicular Technology*, 2010, **59**, (2), pp. 638–649
- Rezaeian, A., Zarringhalam, R., Fallah, S., Melek, W., Khajepour, A., Chen, S.K., et al.: 'Novel tire force estimation strategy for real-time implementation on vehicle applications', *IEEE Transactions on Vehicular Technology*, 2015, **64**, (6), pp. 2231–2241
- Arat, M.A., Singh, K., Taheri, S.: 'Optimal tire force allocation by means of smart tire technology', *SAE Int J Passeng Cars - Mech Syst*, 2013, **6**, pp. 163–176
- Corno, M., Gerard, M., Verhaegen, M., Holweg, E.: 'Hybrid abs control using force measurement', *IEEE Transactions on Control Systems Technology*, 2012, **20**, (5), pp. 1223–1235
- Katriniok, A., Maschuw, J.P., Christen, F., Eckstein, L., Abel, D.: 'Optimal vehicle dynamics control for combined longitudinal and lateral autonomous vehicle guidance', 2013, pp. 17–19
- Kim, D., Kang, J., Yi, K.: 'Control strategy for high-speed autonomous driving in structured road'. In: 14th International IEEE Conference on Intelligent Transportation Systems, Washington, DC, USA, 2011, pp. 5–7
- Noh, K., Jung, D., Choi, H., Yi, K.: 'Development of ergonomic driver model considering human factors'. In: SAE Technical Paper, 2007.
- Xu, J., Yang, K., Shao, Y., Lu, G.: 'An Experimental Study on Lateral Acceleration of Cars in Different Environments in Sichuan, Southwest China', *Discret Dyn Nat Soc*, 2015, pp. 1–16
- The MathWorks, Inc.: 'MATLAB and Simulink product families Release 2015b'. (Natick, Massachusetts), 2016
- Abdul Rachman, A.S., Baldi, S.: 'Integrated vehicle dynamics control: Real-time simulation [video stream]', *YouTube*, 2017, Available from: <https://youtu.be/MBws9cCV5oY>
- Tecnalia Research & Innovation Foundation. 'Dynacar version 1.9'. (San Sebastián, 2016)
- Solyom, S., Idelchi, A., Salamah, B.B.: 'Lateral control of vehicle platoons'. In: 2013 IEEE International Conference on Systems, Man, and Cybernetics, 2013, pp. 4561–4565

9 Appendix

Table 2 Vehicle Parameter

Parameters	Symbol [unit]	Value
Vehicle mass	m [kg]	1.425×10^3
Vehicle maximum speed	v_{max} [m s ⁻¹]	71.111×10^2
Pacejka model coefficients (dry tarmac)		$1.000 \times 10^0,$
		$1.900 \times 10^0,$
	B_p, C_p, D_p, E_p	$1.000 \times 10^0,$
		9.700×10^{-1}
Front wheel axle-CoG distance	l_f [m]	1.240×10^0
Rear wheel axle-CoG distance	l_r [m]	1.460×10^0
Height of CoG	h [m]	6.000×10^{-1}
Vertical axis moment of inertia	I_z [kg m ²]	2.745×10^3
Steering actuator constant	τ_δ [s]	2.000×10^{-1}
Friction coefficient	μ	9.000×10^{-1}
Cornering stiffness	$C_{y,f}$	$3.463 \times 10^4,$
	$C_{y,r}$ [rad ⁻¹]	2.941×10^4

Table 3 Longitudinal Controller Parameter

Parameters	Symbol [unit]	Value
Standstill distance	d_0 [m]	7.70
Desired headway distance time	t_{hw} [s]	1.50
Longitudinal control weight	Q_x	diag(1, 2)
Longitudinal control weight	R_x	32.0
Response delay	τ_h [s]	0.67
Warning index upper threshold	$\bar{\kappa}$	0.20
Warning index lower threshold	$\underline{\kappa}$	0.81
Inverse TTC upper threshold	\bar{T} [s]	1.35
Inverse TTC lower threshold	\underline{T} [s]	0.49

Table 4 Lateral Controller Parameter

Parameters	Symbol [unit]	Value
Medium comfort lateral acceleration	$a_{y,0}$ [m s ⁻²]	3.60
Maximum lateral acceleration	$a_{y,max}$ [m s ⁻²]	7.20
Lateral control weight	Q_y	diag(0, 1, 0, 1, 0.01)
Lateral control weight	R_y	5.00